IEEE Access
Multidisciplinary | Rapid Review | Open Access Journal

Received March 23, 2020, accepted April 15, 2020, date of publication April 23, 2020, date of current version May 11, 2020.

Digital Object Identifier 10.1109/ACCESS.2020.2989783

Dynamic Modeling and Analysis of a 2PRU-UPR Parallel Robot Based on Screw Theory

XINXUE CHAI, MIN WANG, LINGMIN XU, (Member, IEEE), AND WEI YE, (Member, IEEE)
Faculty of Mechanical Engineering and Automation, Zhejiang Sci-Tech University, Hangzhou 301108, China

Corresponding author: Wei Ye (wye@zstu.edu.cn)

This work was supported in part by the National Natural Science Foundation of China under Grant 51705465 and Grant 51935010, and in part by the Natural Science Foundation of Zhejiang Province under Grant LQ19E050015.

ABSTRACT This paper proposes the systemic dynamic modeling and analysis of a 2PRU-UPR parallel robot with two rotations and one translation based on screw theory, where P, R and U denote prismatic, revolute and universal joints, respectively. Compared with existing parallel robots having two rotations and one translation, the two actuated prismatic joints of the 2PRU-UPR parallel robot are mounted on a fixed base to reduce the movable mass and improve the dynamic response. First, the inverse kinematics are presented. Next, adopting the screw-based method, the velocity and acceleration of joints and limbs of the 2PRU-UPR parallel robot are analyzed in detail. The actuated forces of the three actuators are then obtained according to the principle of virtual work. Additionally, a numerical simulation is conducted using ADAMS software to investigate the dynamic model of the 2PRU-UPR manipulator and to verify the correctness of the theoretical results. Finally, distributions of the dynamic manipulability ellipsoid index are used to evaluate the dynamic translational and rotational performances of the 2PRU-UPR parallel robot. A prototype based on the dynamic analysis has been fabricated. The dynamic modeling and evaluation provide a basis for the efficient and precise control of the 2PRU-UPR parallel robot in actual machining manipulations. The 2PRU-UPR parallel robot has great potential in machining workpieces with curved surfaces.

INDEX TERMS Parallel robot, dynamic model, screw theory, dynamic performance.

I. INTRODUCTION

Parallel robots have been intensively studied over past decades and used in many applications, from simple pick-and-place operations to advanced electronic manufacturing [1]–[3]. Having a closed structure, parallel robots have potential advantages of a high load-carrying capacity, good positioning accuracy and low inertia [4]–[7].

Dynamic modeling plays an important role in the pre-design stage of the development of parallel robots and is essential for dynamic performance analysis and parameter optimization. The relations between forces and motions are investigated through modeling [8] [9] and are useful for the development of the control scheme [10], [11]. The dynamic analysis of parallel robots is carried out adopting several methods, mainly the Newton–Euler method [12]–[16], Lagrange method [17]–[21] and the adoption of the virtual work principle [22]–[26]. Additionally, methods such as the use of Gibbs–Appell equations [27], [28] and Kane equation [29], [30] are used in the dynamic analysis of parallel robots.

The Newton–Euler method is the most common approach used in analyzing the dynamic model; it is relatively straightforward to implement and can be understood easily. However, the Newton–Euler method [12]–[16] requires many differential algebraic equations to be established, especially when the parallel system is complex and has multiple constraints. The derivation of equations requires much computational time. In contrast with the Newton–Euler method, the Lagrange method [17]–[21] is based on the kinetic energy and potential energy of the system. The Lagrange method is based on pure mathematics instead of geometry. It is simple to develop the dynamic model with energy and generalized forces. However, a long computational time is required for matrix operations and the derivation of partial differentials. It is noted that the Lagrange method is not good for programming and computation. The use of the virtual work principle [22]–[26] is based on the system's overall virtual energy, which eliminates the

The associate editor coordinating the review of this manuscript and approving it for publication was Vlad Diaconita.

derivation of constrained forces/moments. Such an energy approach for the analysis of a parallel robot can be simplified applying screw theory [31]–[35]. The principle of virtual work is suitable for the programming and computation of parallel robots, including complex models [36]–[38].

Adopting screw theory and the virtual work principle, this paper presents the systemic dynamic modeling and analysis of the three-degree-of-freedom (3-DOF) 2PRU-UPR parallel robot with two rotations and one translation (2R1T) [39]. Compared with existing 2R1T parallel robots, such as the parallel module of the Exechon robot [40], the 2UPR-SPR parallel robot with 13 single-DOF joints, the parallel module of the Tricept robot [41], and the 3UPS-UP parallel robot with 21 single-DOF joints, the 2PRU-UPR parallel robot only has 12 single-DOF joints, which is helpful in terms of decreasing the deformation and clearance caused by the joints [39]. Here, P, R, U and S denote prismatic, revolute, universal and spherical joints, respectively. Additionally, two of actuated prismatic joints of the 2PRU-UPR parallel robot are mounted on a fixed base to reduce the movable mass and improve the dynamic response. In industry, the 2PRU-UPR parallel robot has great potential in machining workpieces with curved surfaces. It is therefore necessary to develop a dynamic model that can be used in further research, such as the design of control systems and experiments. Through screw theory, the expressions of the velocity and acceleration of each joint and limb of the 2PRU-UPR parallel robot are established easily, and these expressions are easy to understand and implement. Using the principle of virtual work, the actuated forces of the 2PRU-UPR parallel robot are obtained directly. The correctness of the theoretical results for a given trajectory is verified by comparing with numerical results obtained using ADAMS software. Using a dynamic model with clear physical meaning and a simple expression allows easier analysis of the dynamic performance of the 2PRU-UPR parallel robot. Additionally, the dynamic model can be used to achieve real-time control with high efficiency and precision, which is beneficial for machining workpieces in industry.

In evaluating the dynamic performance of the 2PRU-UPR parallel robot, the present paper employs the dynamic manipulability ellipsoid (DME) [2], [42]–[44] to depict manipulability, namely the ease with which the position and orientation of the manipulator's moving platform can be changed. The distribution of this index of the 2PRU-UPR parallel robot is obtained and discussed. The results of the paper will serve as criteria for the structural optimization and motion control of a prototype of the 2PRU-UPR parallel robot.

The remainder of the paper is organized as follows. Section 2 briefly introduces the basics of screw theory. Section 3 presents the inverse kinematics analysis. Section 4 analyzes the velocity and acceleration of joints and limbs of the 2PRU-UPR parallel robot. Section 5 presents the derivation of actuated forces and verifies the correctness of the theoretical method. Section 6 presents distributions of the DME for different operating heights. Section 7 describes the prototype and hard system of the 2PRU-UPR parallel robot. Section 8 presents conclusions.

II. SCREW THEORY BASICS

In a Cartesian coordinate system, the position and direction of a line are represented by a vector $\boldsymbol{S}$. $\boldsymbol{r}$ is a position vector at a given point expressed as

$$\boldsymbol{r} \times \boldsymbol{S} = \boldsymbol{S}_0. \tag{1}$$

Equation (1) represents a straight line using homogeneous coordinates $(\boldsymbol{S}; \boldsymbol{S}_0)^T$ to show the position and direction of the line in space. There are six components. The straight line is represented by a screw with the form

$$\$ = (\boldsymbol{S}; \boldsymbol{S}_0)^T = (\boldsymbol{S}; \boldsymbol{r} \times \boldsymbol{S})^T = \begin{pmatrix} L & M & N & p & q & r \end{pmatrix}^T, \tag{2}$$

where $h = \boldsymbol{S} \cdot \boldsymbol{S}_0 / (\boldsymbol{S} \cdot \boldsymbol{S})$ is the pitch of the screw. This screw is a line vector and represents a revolute pair or a binding force when the pitch is zero. A screw with an infinite pitch is expressed as $\$ = (\boldsymbol{0}; \boldsymbol{S})^T$, where $\boldsymbol{S}$ is a direction vector. This screw represents a prismatic pair or a binding couple.

In modeling based on screw theory, the velocity of the rigid body is denoted $\boldsymbol{V}_O$, the primary component is denoted $\vartheta(\boldsymbol{V}_O) = \boldsymbol{\omega}$, and the dual component is denoted $D(\boldsymbol{V}_O) = \boldsymbol{v}_O$. It can be shown that

$$\boldsymbol{V}_O = \begin{bmatrix} \boldsymbol{\omega} & \boldsymbol{v}_O \end{bmatrix}^T, \tag{3}$$

where $\boldsymbol{\omega}$ is the angular velocity of the rigid body and $\boldsymbol{v}_0$ is the linear velocity of point O on the body.

The primary component, $\vartheta(\boldsymbol{V}_O)$, does not change when the position of point O changes. This can be said to be a characteristic of such motion. The dual component, $D(\boldsymbol{V}_O)$, changes accordingly. The speed of a rigid body can be regarded as a twist on a screw, and (3) is thus rewritten as

$$\boldsymbol{V}_O = \omega \$. \tag{4}$$

When the representation point changes from O to P, only the dual part of the twist changes:

$$D(\boldsymbol{V}_P) = \boldsymbol{v}_P = D(\boldsymbol{V}_O) + D(\boldsymbol{V}_O) \times \boldsymbol{r}_{P/O}, \tag{5}$$

where $\boldsymbol{r}_{P/O}$ is the position vector from point O to point P.

From the definition of the screw, $\$ = \begin{bmatrix} \boldsymbol{S} & \boldsymbol{S}_0 \end{bmatrix}^T$, the calculation of $\begin{bmatrix} \$_1 & \$_2 \end{bmatrix}$ is

$$\begin{bmatrix} \$_1 & \$_2 \end{bmatrix}^T = \begin{bmatrix} \boldsymbol{S}_1 \times \boldsymbol{S}_2 \\ \boldsymbol{S}_1 \times \boldsymbol{S}_{02} - \boldsymbol{S}_2 \times \boldsymbol{S}_{01} \end{bmatrix}. \tag{6}$$

III. INVERSE ANALYSIS OF THE 2PRU-UPR PARALLEL ROBOT

To simplify the progress of the dynamic model of the parallel robot, a simplified computer-aided-design model is created as shown in Fig. 1. Here, the moving platform is connected to the fixed base through three kinematic limbs. The first limb, A_1B_1, and the second limb, A_2B_2, are identical PRU kinematic chains. The axis of the R joint is perpendicular to the axis of the P joint, the first axis of the U joint is parallel to the axis

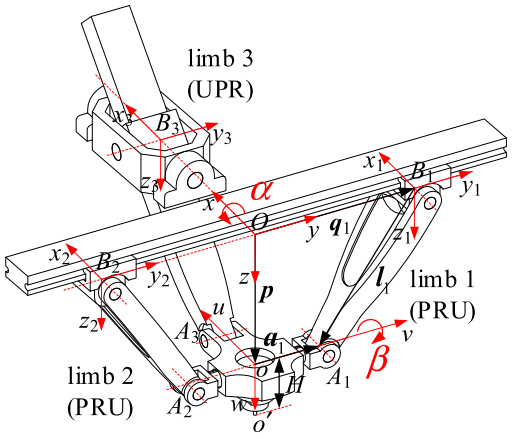

FIGURE 1. 2PRU-UPR parallel robot.

of the R joint, and the second revolute axis of the U joint is connected to the moving platform. The third limb, A_3B_3, is a UPR kinematic chain. The first revolute axis of the U joint is perpendicular to the axis of the P joint. The second revolute axis of the U joint is always parallel to the second axes of the U joints of the first two limbs.

As shown in Fig. 1, the fixed frame $O-xyz$ is attached to the fixed base, and the $x-axis$ and $y-axis$ pass through points B_3 and B_1, respectively. A moving frame $o-uvw$ is attached to the moving platform with $u-axis$ along oA_3 and $v-axis$ along oA_1. The local coordinate frame of each limb, as shown in Fig. 1, is established to describe inertial characteristics. The local coordinate frames $B_i-x_{ij}y_{ij}z_{ij}$ are attached to the kinematic links of the 2PRU-UPR parallel robot. The dimensional parameters of the 2PRU-UPR parallel robot are defined as $A_1B_1 = l_1$, $A_2B_2 = l_2$, $oA_2 = a_2$, $oA_3 = a_3$, $oB_3 = b_3$ and $oo' = H$.

According to Fig. 1, the closed-loop vector equation of the 2PRU-UPR parallel robot can be written as $\boldsymbol{p} + \boldsymbol{a}_i = \boldsymbol{q}_i + \boldsymbol{l}_i$, where vector $\boldsymbol{a}_i = a_i\boldsymbol{e}_i$ denotes oA_i and $\boldsymbol{e}_1 = \begin{bmatrix} 0 & 1 & 0 \end{bmatrix}^T$, $\boldsymbol{e}_2 = \begin{bmatrix} 0 & -1 & 0 \end{bmatrix}^T$ and $\boldsymbol{e}_3 = \begin{bmatrix} 1 & 0 & 0 \end{bmatrix}^T$. $\boldsymbol{q}_i$ is the vector of the actuated joint, and $\boldsymbol{q}_1 = OB_1$, $\boldsymbol{q}_2 = OB_2$ and $\boldsymbol{q}_3 = B_3A_3$. $\boldsymbol{l}_1, \boldsymbol{l}_2$ and $\boldsymbol{l}_3$ are vectors of links A_1B_1, A_2B_2 and OB_3, respectively.

To simplify the dynamic analysis of the 2PRU-UPR parallel robot, $\boldsymbol{\eta} = \begin{bmatrix} z & \alpha & \beta \end{bmatrix}^T$ is chosen as the vector of independent generalized coordinates in this paper. The dependent coordinates must satisfy the constraints

$$\begin{cases} \gamma = 0 \\ x = 0 \\ y = z\tan(\alpha) \end{cases}, \tag{7}$$

where γ denotes the rotation angle around the z-axis and the term tan denotes the tangent function. As shown in Fig. 1, $\boldsymbol{p} = \begin{bmatrix} 0 & z_o\tan\alpha & z_o \end{bmatrix}^T$, $\boldsymbol{b}_1 = \begin{bmatrix} 0 & q_1 & 0 \end{bmatrix}^T$, $\boldsymbol{b}_2 = \begin{bmatrix} 0 & -q_2 & 0 \end{bmatrix}^T$ and $\boldsymbol{b}_3 = \begin{bmatrix} b_3 & 0 & 0 \end{bmatrix}^T$.

According to [38], the inverse kinematics of the 2PRU-UPR parallel robot are written as

$$\begin{cases} q_1 = \sqrt{l_1^2 - (z - a_1s\alpha)^2} + a_1c\alpha + z\tan(\alpha) \\ q_2 = \sqrt{l_1^2 - (z + a_1s\alpha)^2} + a_1c\alpha - z\tan(\alpha) \\ q_3 = \sqrt{(z/c\alpha - a_3s\beta)^2 + (a_3c\beta - b_3)^2}. \end{cases} \tag{8}$$

IV. VELOCITY AND ACCELERATION ANALYSIS OF THE 2PRU-UPR PARALLEL ROBOT

The generalized velocity of the moving platform is obtained by taking derivatives of (7):

$$\begin{cases} \dot{\gamma} = 0 \\ \dot{x} = 0 \\ \dot{y} = z\sec^2(\alpha)\dot{\alpha} + \dot{z}\tan(\alpha) \\ \quad = \tan(\alpha)\dot{z} + z\sec^2(\alpha)\dot{\alpha} \end{cases} \tag{9}$$

The linear velocity and rotational velocity of the moving platform are therefore

$$\boldsymbol{t_p} = \begin{pmatrix} \boldsymbol{\omega}_P^T & \boldsymbol{v}_P^T \end{pmatrix} = \boldsymbol{K}_p\dot{\boldsymbol{\eta}}, \tag{10}$$

where $\boldsymbol{v}$ and $\boldsymbol{\omega}$ are the linear velocity and rotational velocity of a given point P on the moving platform and $\boldsymbol{K}_p$ is the mapping between the velocity of the moving platform and the generalized coordinates. $\boldsymbol{K}_p$ is expressed as

$$\boldsymbol{K}_p = \begin{bmatrix} 0 & 0 & 0 & 0 & \tan(\alpha) & 1 \\ c\beta & 0 & -s\beta & 0 & z\sec^2(\alpha) & 0 \\ 0 & 1 & 0 & 0 & 0 & 0 \end{bmatrix}^T. \tag{11}$$

The linear velocity and rotational velocity are differentiated to obtain the linear acceleration and rotational acceleration of the moving platform:

$$\dot{\boldsymbol{t}}_{\boldsymbol{p}} = \boldsymbol{K}_p\ddot{\boldsymbol{\eta}} + \dot{K}_p\dot{\boldsymbol{\eta}}. \tag{12}$$

Here, the first limb (i.e., the PRU limb) is taken as an example to verify the proposed method. With respect to the fixed frame $O-xyz$, the twist system of the first limb in the fixed frame $O-xyz$ is written as

$$\begin{cases} \$_{11} = \begin{pmatrix} 0 & 0 & 0; & 0 & 1 & 0 \end{pmatrix} \\ \$_{12} = \begin{pmatrix} 1 & 0 & 0; & 0 & 0 & -q_1 \end{pmatrix} \\ \$_{13} = \begin{pmatrix} 1 & 0 & 0; & 0 & z - a_1s\alpha & -y - a_1c\alpha \end{pmatrix} \\ \$_{14} = \begin{pmatrix} 0 & c\alpha & -s\alpha; & -zc\alpha - ys\alpha & 0 & 0 \end{pmatrix} \end{cases} \tag{13}$$

The corresponding twist system of the first limb is rewritten as a 6×1 matrix and the velocity of the rigid body is written as

$$\boldsymbol{V_0} = \begin{bmatrix} \boldsymbol{\omega} & \boldsymbol{v_0} \end{bmatrix}^T. \tag{14}$$

In the case of the 2PRU-UPR parallel robot, the linear expression of the moving platform is

$${}^0\vec{\boldsymbol{V}}^4 = {}_0\omega_1^i\ \$_{i1} + {}_1\omega_2^i\ \$_{i2} + {}_2\omega_3^i\ \$_{i3} + {}_3\omega_4^i\ \$_{i4}, \quad i = 1, 2, 3. \tag{15}$$

The linear velocity and rotational velocity of the moving platform are expressed according to (5) as

$$ {}^{0}\boldsymbol{V}^{4} = \begin{bmatrix} \boldsymbol{\omega} \\ v_0 + \boldsymbol{\omega} \times r_{po} \end{bmatrix} = \begin{bmatrix} \omega^T & v^T \end{bmatrix}^T. \tag{16} $$

Equation (16) is written in matrix form as

$$ {}^{0}\boldsymbol{V}^{4} = J_i \begin{bmatrix} {}_0\omega_1^i & {}_1\omega_2^i & {}_2\omega_3^i & {}_3\omega_4^i \end{bmatrix}^T, \tag{17} $$

where $\boldsymbol{J}_i = \begin{bmatrix} \$_{i1} & \$_{i2} & \$_{i3} & \$_{i4} \end{bmatrix}$ is a 6×4 Jacobian matrix. Using (13), the Jacobian matrix of the first limb is obtained as

$$ \begin{aligned} \boldsymbol{J}_1 &= \begin{bmatrix} \$_{11} & \$_{12} & \$_{13} & \$_{14} \end{bmatrix} \\ &= \begin{bmatrix} 0 & 1 & 1 & 0 \\ 0 & 0 & 0 & c\alpha \\ 0 & 0 & 0 & -s\alpha \\ 0 & 0 & 0 & -zc\alpha - ys\alpha \\ 1 & 0 & z - a_1 s\alpha & 0 \\ 0 & -q_1 & -y - a_1 c\alpha & 0 \end{bmatrix}. \end{aligned} \tag{18} $$

The velocity of the moving platform, relative to the fixed link, was solved as (17). The Jacobian matrix of the mechanism is reversible if the mechanism does not have motion redundancy. The rotational velocity ${}_i\omega_{i+1}$ is obtained by inversing the Jacobian matrix $\boldsymbol{J}_i$:

$$ \begin{bmatrix} {}_0\omega_1^i \\ {}_1\omega_2^i \\ {}_2\omega_3^i \\ {}_3\omega_4^i \end{bmatrix} = \begin{bmatrix} \$_{i1}^T & \$_{i2}^T & \$_{i3}^T & \$_{i4}^T \end{bmatrix}^{-1} \begin{bmatrix} \boldsymbol{\omega}^T & \boldsymbol{v}^T \end{bmatrix}^T. \tag{19} $$

We define a unit screw $\$_{unit}^{(i)}$, which is rewritten as a 6×1 matrix. According to the structural parameters of the 2PRU-UPR parallel robot, the unit screw $\$_{unit}^{(i)}$ intersects all screw vectors except the prismatic pair of the *ith* limb, such that the reciprocal product of the unit screw $\$_{unit}^{(i)}$ and all the screws of the *ith* limb except the prismatic pair screw is zero. This is expressed as

$$ KL(\$_{unit}^{(i)}, {}^{j}\$^{j+1}) = 0, \quad j = 1, 2, 3, \tag{20} $$

where ${}^{j}\$^{j+1}$ denotes all screws of the *ith* limb except the prismatic pair screw. The Klein form is applied to both sides of (20).

The relationship between the drive velocity of each limb and the velocity of the moving platform is written as

$$ \dot{\boldsymbol{q}}_i = KL\left(\$_{unit}^{(i)}, {}^{0}\vec{\boldsymbol{V}}^{4}\right) = \frac{\$_{unit}^{(i)} \Delta {}^{0}\vec{\boldsymbol{V}}^{4}}{\$_{unit}^{(i)} \Delta \$_i^q} = \$^{(i)} \Delta {}^{0}\vec{\boldsymbol{V}}^{4}, \tag{21} $$

where $\Delta = \begin{bmatrix} \boldsymbol{0}_{3\times3} & \boldsymbol{I}_3 \\ \boldsymbol{I}_3 & \boldsymbol{0}_{3\times3} \end{bmatrix} = \Delta^{-1}$.

Substituting (16) into (21) yields

$$ \dot{\boldsymbol{q}}_i = \begin{bmatrix} \dot{q}_1 \\ \dot{q}_2 \\ \dot{q}_3 \end{bmatrix} = \begin{bmatrix} \$^{(1)T} \Delta {}^{0}\vec{\boldsymbol{V}}^{4} \\ \$^{(2)T} \Delta {}^{0}\vec{\boldsymbol{V}}^{4} \\ \$^{(3)T} \Delta {}^{0}\vec{\boldsymbol{V}}^{4} \end{bmatrix} = \boldsymbol{J}_s^T \Delta \boldsymbol{J}_i \boldsymbol{J}_\omega^i, \tag{22} $$

where $\boldsymbol{J}_s = \begin{bmatrix} \$^{(1)^T} & \$^{(2)^T} & \$^{(3)^T} \end{bmatrix}, \boldsymbol{J}_\omega^i = \begin{bmatrix} {}_0\omega_1^i & {}_1\omega_2^i & {}_2\omega_3^i & {}_3\omega_4^i \end{bmatrix}^T$.

Here, $\boldsymbol{J}_\omega^i$ is a joint velocity matrix for the *ith* limb. The drive velocity of the *ith* limb is obtained using (22) and the velocity of the moving platform. Rearranging (22) gives

$$ \boldsymbol{J}_\omega^i = \left(\boldsymbol{J}_s^T \Delta \boldsymbol{J}_i\right)^{-1} \dot{\boldsymbol{q}}_i. \tag{23} $$

We define a coefficient $\boldsymbol{G}_{k\omega_{k+1}}^{j}$ for the relation between the velocity of active joint j and the rotational velocity of passive joint k and obtain

$$ {}_k\omega_{k+1} = \boldsymbol{G}_{k\omega_{k+1}}^{1} \dot{q}_1 + \boldsymbol{G}_{k\omega_{k+1}}^{2} \dot{q}_2 + \boldsymbol{G}_{k\omega_{k+1}}^{3} \dot{q}_3. \tag{24} $$

Substituting (24) into (23) yields

$$ \begin{bmatrix} {}_0\omega_1^i \\ {}_1\omega_2^i \\ {}_2\omega_3^i \\ {}_3\omega_4^i \end{bmatrix} = \begin{bmatrix} G^1_{{}_0\omega_1^i} & G^2_{{}_0\omega_1^i} & G^3_{{}_0\omega_1^i} \\ G^1_{{}_1\omega_2^i} & G^2_{{}_1\omega_2^i} & G^3_{{}_1\omega_2^i} \\ G^1_{{}_2\omega_3^i} & G^2_{{}_2\omega_3^i} & G^3_{{}_2\omega_3^i} \\ G^1_{{}_3\omega_4^i} & G^2_{{}_3\omega_4^i} & G^3_{{}_3\omega_4^i} \end{bmatrix} \begin{bmatrix} \dot{q}_1 \\ \dot{q}_2 \\ \dot{q}_3 \end{bmatrix}. \tag{25} $$

Equation (25) shows that the joint rotational velocity of the corresponding limb is derived from the driving velocity and coefficient $\boldsymbol{G}_{k\omega_{k+1}}^{j}$. We define $\$_n^{ji} = G^{j}_{{}_0\omega_1^i}\ \$_{i1} + \ldots + G^{j}_{{}_{n-1}\omega_n^i}\ \$_{in}$. Substituting (25) into (17) yields

$$ \begin{aligned} {}^{0}\vec{\boldsymbol{V}}^{n(i)} &= \left(G^1_{{}_0\omega_1^i}\ \$_{i1} + \ldots + G^1_{{}_{n-1}\omega_n^i}\ \$_{in}\right) \dot{q}_1 \\ &\quad + \left(G^2_{{}_0\omega_1^i}\ \$_{i1} + \cdots + G^2_{{}_{n-1}\omega_n^i}\ \$_{in}\right) \dot{q}_2 \\ &\quad + \left(G^3_{{}_0\omega_1^i}\ \$_{i1} + \cdots + G^3_{{}_{n-1}\omega_n^i}\ \$_{in}\right) \dot{q}_3. \end{aligned} \tag{26} $$

The vector of the centroid of link C_m is denoted, with respect to its own coordinate system, as $\boldsymbol{r}_o$. With respect to the base coordinate system, the centroid of link C_m is expressed as $\boldsymbol{r}_n = \boldsymbol{R}_{Li}\boldsymbol{r}_o$. The centroid velocity screw of the component is

$$ \boldsymbol{V}_{nCm}^{i} = \sum_{j=1}^{3} \left(\begin{bmatrix} \vartheta(\$_n^{ji}) \\ D(\$_n^{ji}) + \vartheta(\$_n^{ji}) \times \vec{\boldsymbol{r}}_{n(i)} \end{bmatrix} \dot{q}_j \right). \tag{27} $$

We define the centroid partial screw of a component as

$$ \$_{nCm(i)}^{j} = \begin{bmatrix} \vartheta(\$_n^{ji}) \\ D(\$_n^{ji}) + \vartheta(\$_n^{ji}) \times \vec{\boldsymbol{r}}_{n(i)} \end{bmatrix}. \tag{28} $$

We denote the acceleration of the rigid body by $\boldsymbol{A}_o$, denote the primary component by $\vartheta(\boldsymbol{A}_O) = \dot{\boldsymbol{\omega}}$, and express the dual component as $D(\boldsymbol{A}_O) = \boldsymbol{a}_0 - \boldsymbol{\omega} \times \boldsymbol{v}_O$; i.e.,

$$ \boldsymbol{A}_O = \begin{bmatrix} \dot{\boldsymbol{\omega}} \\ \boldsymbol{a}_0 - \boldsymbol{\omega} \times \boldsymbol{v}_O \end{bmatrix}, \tag{29} $$

where $\dot{\boldsymbol{\omega}}$ is the angular velocity and $\boldsymbol{a}_0 - \boldsymbol{\omega} \times \boldsymbol{v}_O$ is the linear acceleration of the rigid body at point O. Applying the theory of primary kinematics, the acceleration of the given point P is obtained as

$$ \begin{aligned} \boldsymbol{A}_P &= \begin{bmatrix} \dot{\boldsymbol{\omega}} & \boldsymbol{a}_P - \boldsymbol{\omega} \times \boldsymbol{v}_P \end{bmatrix}^T \\ &= \begin{bmatrix} \dot{\boldsymbol{\omega}} & \boldsymbol{a}_O + \dot{\boldsymbol{\omega}} \times \boldsymbol{r}_{P/O} + \boldsymbol{\omega} \times \left(\boldsymbol{\omega} \times \boldsymbol{r}_{P/O}\right) - \boldsymbol{\omega} \times \boldsymbol{v}_P \end{bmatrix}^T. \end{aligned} \tag{30} $$

A reference coordinate system is attached to the fixed link, such that the acceleration of the moving part m relative to the fixed link is derived as

$$ {}^{0}\boldsymbol{A}^{m}=\begin{bmatrix}\dot{\boldsymbol{\omega}}_m\\ \boldsymbol{a}_m\end{bmatrix}={}_0\dot{\omega}_1\,\$_1+{}_1\dot{\omega}_2\,\$_2+\ldots+{}_{m-1}\dot{\omega}_m\,\$_m+\$_{\mathrm{L}}, \tag{31} $$

where

$$ \begin{aligned}\$^i_{\mathrm{L}}=&\begin{bmatrix}{}_0\boldsymbol{\omega}^i_1 & \$_{i1} & {}_1\boldsymbol{\omega}^i_2 & \$_{i2} & {}_2\boldsymbol{\omega}^i_3 & \$_{i3} & {}_3\boldsymbol{\omega}^i_4 & \$_{i4}\end{bmatrix}\\ &+\begin{bmatrix}{}_0\boldsymbol{\omega}^i_1 & \$_{i1} & {}_1\boldsymbol{\omega}^i_2 & \$_{i2} & {}_2\boldsymbol{\omega}^i_3 & \$_{i3} & {}_3\boldsymbol{\omega}^i_4 & \$_{i4}\end{bmatrix}\\ &+\begin{bmatrix}{}_0\boldsymbol{\omega}^i_1 & \$_{i1} & {}_1\boldsymbol{\omega}^i_2 & \$_{i2} & {}_2\boldsymbol{\omega}^i_3 & \$_{i3} & {}_3\boldsymbol{\omega}^i_4 & \$_{i4}\end{bmatrix}.\end{aligned} $$

The reciprocal product of two screws $\begin{bmatrix}\$_1 & \$_2\end{bmatrix}$ was introduced in (6). When the mechanism does not have motion redundancy, the Jacobian matrix of the mechanism is reversible, and (31) is rewritten as

$$ \begin{bmatrix}{}_0\omega^i_1 & {}_1\omega^i_2 & {}_2\omega^i_3 & {}_3\omega^i_4\end{bmatrix}^T=\boldsymbol{J}_i^{-1}\left({}^{0}\mathbf{A}^4-\$^i_L\right). \tag{32} $$

The corresponding value of screw $\$_L$ based on (32) is a 6×1 matrix. According to (29), the acceleration of the rigid body is

$$ \boldsymbol{a}_0=D(\boldsymbol{A}_O)+\boldsymbol{\omega}\times\boldsymbol{v}_O. \tag{33} $$

According to (30), the acceleration of the link in the 2PRU-UPR parallel robot is

$$ \boldsymbol{a}=\boldsymbol{a}_0+\dot{\boldsymbol{\omega}}\times\boldsymbol{r}_O+\boldsymbol{\omega}\times(\boldsymbol{\omega}\times\boldsymbol{r}_O). \tag{34} $$

The centroid acceleration of the moving platform and sliders is

$$ \begin{cases}\boldsymbol{A}^i_{sCm}=\begin{bmatrix}\dot{\boldsymbol{\omega}}^i_{sCm}\\ \boldsymbol{a}^i_{sCm}\end{bmatrix}\\ \quad=\begin{bmatrix}\dot{\boldsymbol{\omega}}^i_s\\ \boldsymbol{a}^i_{s0}+\dot{\boldsymbol{\omega}}^i_s\times\boldsymbol{r}^i_1+\boldsymbol{\omega}^i_s\times\left(\boldsymbol{\omega}^i_s\times\boldsymbol{r}^i_1\right)\end{bmatrix}, \quad i=1,2\\ \boldsymbol{A}_{pCm}=\begin{bmatrix}\dot{\boldsymbol{\omega}}_{pCm}\\ \boldsymbol{a}_{pCm}\end{bmatrix}\\ \quad=\begin{bmatrix}\dot{\omega}_P\\ \boldsymbol{a}_{P0}+\dot{\boldsymbol{\omega}}_P\times\boldsymbol{r}_{P0}+\boldsymbol{\omega}_P\times(\boldsymbol{\omega}_P\times\boldsymbol{r}_{P0})\end{bmatrix}.\end{cases} \tag{35} $$

The centroid acceleration of the links is

$$ \begin{cases}\boldsymbol{A}^i_{lCm}=\begin{bmatrix}\dot{\boldsymbol{\omega}}^i_{lCm}\\ \boldsymbol{a}^i_{lCm}\end{bmatrix}=\begin{bmatrix}\dot{\boldsymbol{\omega}}^i_l\\ \boldsymbol{a}^i_{l0}+\dot{\boldsymbol{\omega}}^i_l\times\boldsymbol{r}^i_2+\boldsymbol{\omega}^i_l\times\left(\boldsymbol{\omega}^i_l\times\boldsymbol{r}^i_2\right)\end{bmatrix},\\ \qquad i=1,2\\ \boldsymbol{A}^i_{lCm}=\begin{bmatrix}\dot{\boldsymbol{\omega}}^i_{lCm}\\ \boldsymbol{a}^i_{lCm}\end{bmatrix}=\begin{bmatrix}\dot{\boldsymbol{\omega}}^i_l\\ \boldsymbol{a}^i_{l0}+\dot{\boldsymbol{\omega}}^i_l\times\boldsymbol{r}^i_3+\boldsymbol{\omega}^i_l\times\left(\boldsymbol{\omega}^i_l\times\boldsymbol{r}^i_3\right)\end{bmatrix},\\ \qquad i=3.\end{cases} \tag{36} $$

V. FORCE ANALYSIS AND NUMERICAL SIMULATION

Different limbs have similar compositions and can be regarded as having the same structure. The external force $\boldsymbol{F}_O$ acting on the rigid body can be defined as a screw with basic elements, where $\vartheta(\boldsymbol{F}_O)=\vec{f}$, $D(\boldsymbol{F}_O)=\vec{\tau}_o$, and $\vec{f}$ and $\vec{\tau}_o$ denote the force screw and torque screw acting on point O, respectively. The external force $\boldsymbol{F}_O$ can therefore be written as

$$ \boldsymbol{F}_O=\begin{bmatrix}\vec{f}\\ \vec{\tau}_O\end{bmatrix}. \tag{37} $$

We use ${}^{0}\boldsymbol{V}^n_{Cm}$ and ${}^{0}\boldsymbol{A}^n_{Cm}$ to denote the velocity and acceleration of a centroid C_m of a rigid body whose mass is m, respectively. We assume a force $\boldsymbol{F}^n_{I,Cm}$ acting on the center of mass C_m:

$$ \vec{\boldsymbol{F}}^n_{I,Cm}=\begin{bmatrix}-m\vec{\boldsymbol{a}}_{cm}\\ -\boldsymbol{I}_n\dot{\vec{\boldsymbol{\omega}}}-\vec{\boldsymbol{\omega}}\times\boldsymbol{I}_n\boldsymbol{\omega}\end{bmatrix}, \tag{38} $$

where $\boldsymbol{I}_n={}^{0}\boldsymbol{R}^n\boldsymbol{I}^{\circ}_n\left({}^{0}\boldsymbol{R}^n\right)^T$ is the inertia of the link with respect to the base coordinate system.

Denoting the acceleration due to gravity by $\vec{\boldsymbol{g}}$, the force $\boldsymbol{F}^n_{G,Cm}$ is written as

$$ \vec{\boldsymbol{F}}^n_{G,Cm}=\begin{bmatrix}m\vec{\boldsymbol{g}}\\ \vec{\mathbf{0}}\end{bmatrix}. \tag{39} $$

Assuming that an external force $\vec{\boldsymbol{f}}^n_E$ and torque $\vec{\boldsymbol{\tau}}^n_E$ act at the center of mass of the link, the external force $\vec{\boldsymbol{F}}^n_{E,Cm}$ is written as

$$ \vec{\boldsymbol{F}}^n_{E,Cm}=\begin{bmatrix}\vec{\boldsymbol{f}}^n_E\\ \vec{\boldsymbol{\tau}}^n_E\end{bmatrix}. \tag{40} $$

In the dynamic equations of the mechanism, the force of each link must be based on the same coordinate system. The vector of force $\vec{\boldsymbol{F}}^n$ acting on a link is written as

$$ \vec{\boldsymbol{F}}^n=\vec{\boldsymbol{F}}^n_{I,Cm}+\vec{\boldsymbol{F}}^n_{G,Cm}+\vec{\boldsymbol{F}}^n_{E,Cm}. \tag{41} $$

The instantaneous power ω_n acting on the mass center of the link is expressed as

$$ \omega_n=KL(\vec{\boldsymbol{F}}^n,{}^{0}\boldsymbol{V}^n_{Cm}). \tag{42} $$

In the case of the 2PRU-UPR parallel robot, the force screw acting on the moving platform and the sliders is

$$ \begin{cases}\boldsymbol{F}_p=\begin{bmatrix}m_p\left(\boldsymbol{g}-\boldsymbol{a}_{pCm}\right)\\ -\boldsymbol{I}_P\dot{\boldsymbol{\omega}}_{pCm}-\boldsymbol{\omega}_p\times\boldsymbol{I}_P\boldsymbol{\omega}_p\end{bmatrix}\\ \boldsymbol{F}^{s(\mathrm{i})}=\begin{bmatrix}m^{(i)}_s(\boldsymbol{g}-\boldsymbol{a}^i_{sCm})\\ -\boldsymbol{I}^{(i)}_s\dot{\boldsymbol{\omega}}^i_{sCm}-\boldsymbol{\omega}^i_{sCm}\times\boldsymbol{I}^{(i)}_s\boldsymbol{\omega}^i_{sCm}\end{bmatrix}, \quad i=1,2.\end{cases} \tag{43} $$

The force screw acting on the link is

$$ \begin{cases}\boldsymbol{F}^{\mathrm{l}(i)}=\begin{bmatrix}m^{(i)}_l(\boldsymbol{g}-\boldsymbol{a}^i_{lCm})\\ -\boldsymbol{I}^{(i)}_l\dot{\boldsymbol{\omega}}^i_{lCm}-\boldsymbol{\omega}^i_{lCm}\times\boldsymbol{I}^{(i)}_l\boldsymbol{\omega}^i_{lCm}\end{bmatrix}, \quad i=1,2\\ \boldsymbol{F}^{\mathrm{l}(i)}=\begin{bmatrix}m^{(i)}_l(\boldsymbol{g}-\boldsymbol{a}^i_{lCm})\\ -\boldsymbol{I}^{(i)}_l\dot{\boldsymbol{\omega}}^i_{lCm}-\boldsymbol{\omega}^i_{lCm}\times\boldsymbol{I}^{(i)}_l\boldsymbol{\omega}^i_{lCm}\end{bmatrix}, \quad i=3.\end{cases} \tag{44} $$

Here, m_l, m_s and m_p are the masses of the corresponding links, sliders, and moving platform, respectively. Parameter $\boldsymbol{g}$ denotes gravity. Parameters I_s, I_l and I_P denote the moments of inertia of the corresponding links, sliders and moving platform, respectively. The driving force is calculated using (41) and the principle of virtual work:

$$\begin{aligned} W = &\sum_{v=1}^{3}\left(KL(\boldsymbol{F}^{s(1)}, \boldsymbol{V}^{v}_{1Cm}) + KL(\boldsymbol{F}^{p}, \boldsymbol{V}^{v}_{4Cm})\right) \\ &+ \sum_{v=1}^{3}\left(KL(\boldsymbol{F}^{l(1)}, \boldsymbol{V}^{v}_{2Cm}) + KL(\boldsymbol{F}^{l(2)}, \boldsymbol{V}^{v}_{2Cm})\right) \\ &+ \sum_{v=1}^{3}\left(\boldsymbol{\tau}_v\dot{q}_v + KL(\boldsymbol{F}^{l(3)}, \boldsymbol{V}^{v}_{3Cm})\right). \end{aligned} \tag{45}$$

The principle of virtual work is that for any virtual displacement, the sum of virtual work done by external forces and internal forces of a multi-rigid body system under the effect of an external drive is zero. The virtual velocity $\delta\dot{q}_i$ is substituted into (45) to give

$$\begin{aligned} &\delta W \\ &= \sum_{j=1}^{3}\left(KL(\boldsymbol{F}^{s(1)}, \boldsymbol{\$}^{j}_{1Cm(1)}) + KL(\boldsymbol{F}^{s(2)}, \boldsymbol{\$}^{j}_{1Cm(2)})\right)\delta\dot{q}_j \\ &\quad + \sum_{j=1}^{3}\left(KL(\boldsymbol{F}^{l(1)}, \boldsymbol{\$}^{j}_{2Cm(1)}) + KL(\boldsymbol{F}^{l(2)}, \boldsymbol{\$}^{j}_{2Cm(2)})\right)\delta\dot{q}_j \\ &\quad + \sum_{j=1}^{3}\left(KL(\boldsymbol{F}^{l(3)}, \boldsymbol{\$}^{j}_{3Cm(3)}) + KL(\boldsymbol{F}^{p}, \boldsymbol{\$}^{j}_{4Cm(1)}) + \tau_j\right)\delta\dot{q}_j. \end{aligned} \tag{46}$$

For an arbitrary choice of the virtual velocity $\delta\dot{q}_i$, the total virtual work is zero. $\delta W = 0$ if and only if

$$\begin{aligned} \tau_j = &-\boldsymbol{F}^{s(1)}\Delta\ \boldsymbol{\$}^{j}_{1Cm(1)} - \boldsymbol{F}^{s(2)}\Delta\ \boldsymbol{\$}^{j}_{1Cm(2)} - \boldsymbol{F}^{l(1)}\Delta\ \boldsymbol{\$}^{j}_{2Cm(1)} \\ &- \boldsymbol{F}^{l(2)}\Delta\ \boldsymbol{\$}^{j}_{2Cm(2)} - \boldsymbol{F}^{l(3)}\Delta\ \boldsymbol{\$}^{j}_{3Cm(3)} - \boldsymbol{F}^{p}\Delta\ \boldsymbol{\$}^{j}_{4Cm(1)}, \end{aligned} \tag{47}$$

and the drive can be obtained.

Equation (47) solves out the drive of the 2PRU-UPR parallel robot. The drive of the mechanism is derived through the given mechanism model parameters and the track of the moving platform. We import the model into ADAMS software for simulation. Finally, the simulation results of ADAMS are verified with the calculated drive values.

In the numerical calculation, the lengths of the first and second limbs are $l_1 = l_2 = 0.259m$, the dimensions of the moving platform are $a_1 = a_2 = 0.074m$, and the distance of the sub-center U of the third limb from the origin of the fixed coordinate system is $b_3 = 0.148m$. Other structural parameters are listed in Table 1. The trajectories are tested for the dynamic model

$$\alpha = \arctan\frac{0.015\sin(\pi t)}{0.15{+}0.03\pi t}$$

TABLE 1. Parameters of the parallel robot.

Parts	Mass (kg)	Centroid (mm)	Moment of inertia (kg·mm)
Slider	1	[0 −0.257 −19.408]	[35.922 39.370 53.773]
Link 1 and 2	5	[0 0 128.556]	[2475.147 2472.760 101.114]
Link 3	10	[0 0 160.704]	[3530.345 3529.353 78.770]
Moving platform	20	[2.166 0 2.615]	[3380.754 4876.097 2109.679]

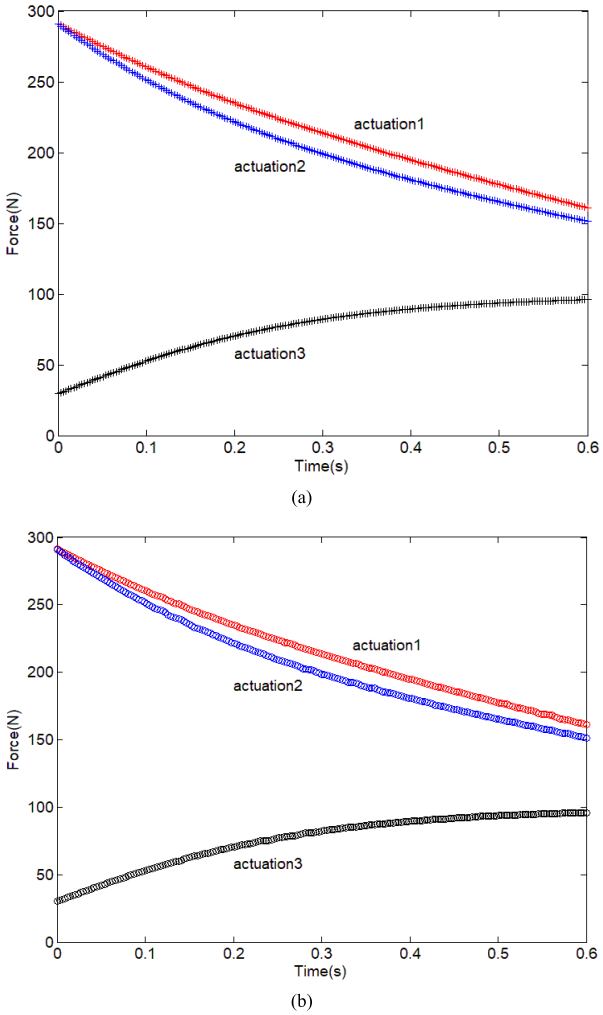

FIGURE 2. Comparison of driving forces of the 2PRU-UPR parallel robot obtained using the proposed method and ADAMS. (a) Driving forces of actuations 1, 2, and 3 by using the screw theory. (b) Driving forces of actuation 1, 2, and 3 by using the ADAMS simulation.

$$\begin{aligned} \beta &= \arcsin\frac{0.015\cos(\pi t)}{0.049} \\ z &= 0.15{+}0.03\pi t - 0.049\cos\alpha\cos\beta, \end{aligned} \tag{48}$$

where t is time. The duration of simulation is set at 0.6s.

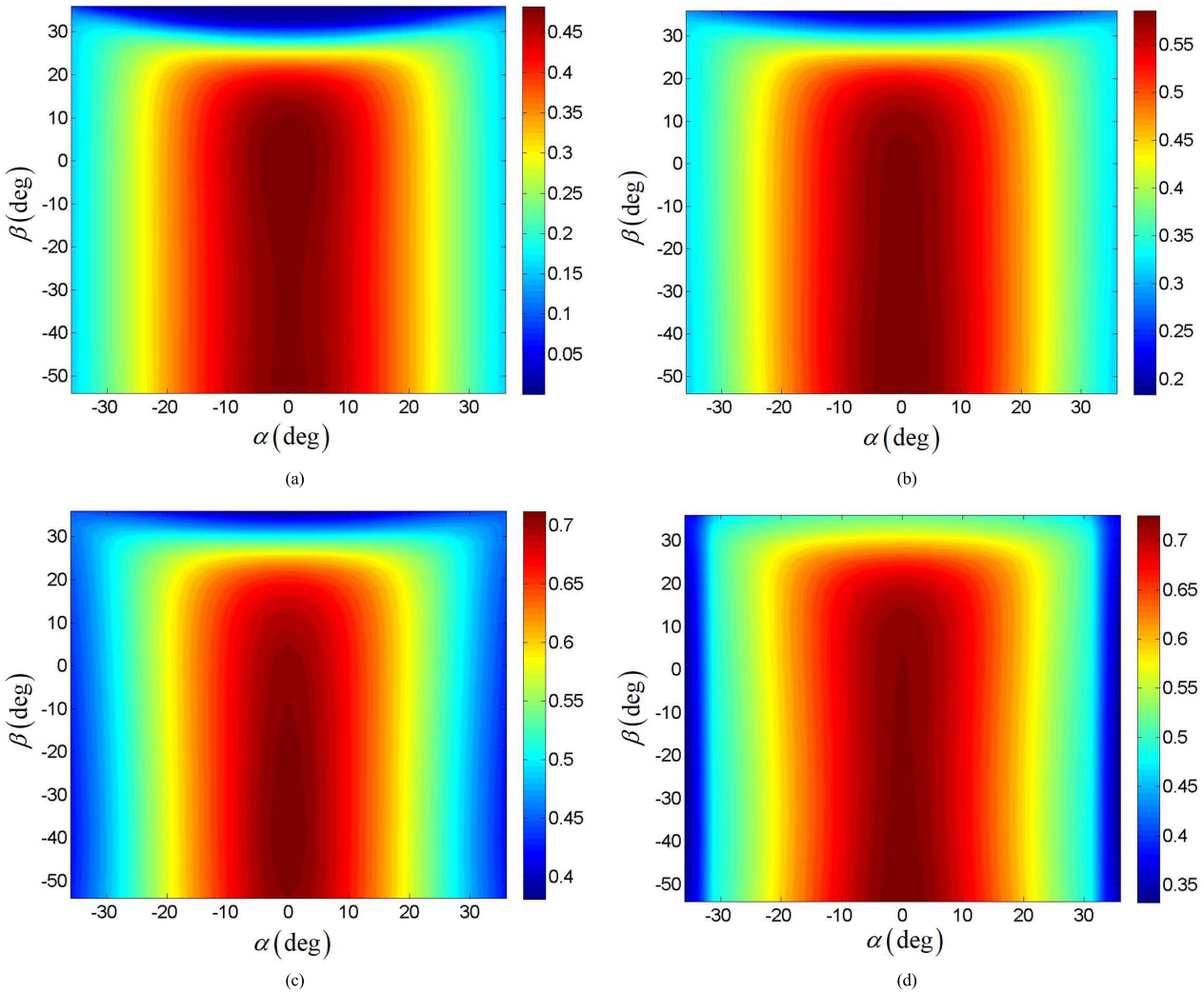

FIGURE 3. Dynamic index of translation for different values of z. (a) DME for translation with $z = 0.1$ m. (b) DME for translation with $z = 0.14$ m. (c) DME for translation with $z = 0.18$ m. (d) DME for translation with $z = 0.22$ m.

Given the trajectory (48) of the moving platform, the driving forces of prismatic joints are calculated from the above dynamic analysis. Figure 2 shows that the driving forces of the 2PRU-UPR parallel robot obtained using the proposed method and ADAMS are almost the same. The proposed theoretical dynamic model can therefore be regarded as an alternative for the accurate dynamic modeling of the 2PRU-UPR parallel robot.

VI. DYNAMIC PERFORMANCE ANALYSIS OF THE 2PRU-UPR PARALLEL ROBOT

This section uses the DME method [2], [42]–[44] to evaluate the dynamic performance of the 2PRU-UPR parallel robot. By ignoring the effects of velocity and gravity on the actuated forces, this method develops the mapping relationship between the acceleration of the moving platform and actuated forces, from which the dynamic performance of the 2PRU-UPR parallel robot can be evaluated. Additionally, by separating the Jacobian matrix, the DME method can be adopted to analyze the accelerations of translation and rotation of the moving platform under a driving force for prismatic joints. This section also derives distributions of DME indices in the workspace for different operational heights. These dynamic analyses will be useful for the control and experiments of the 2PRU-UPR parallel robot in future work.

The system equation of motion of the parallel manipulator is

$$\boldsymbol{\tau} = \boldsymbol{M}(q)\ddot{\boldsymbol{q}} + \boldsymbol{C}(q, \dot{q})\dot{\boldsymbol{q}} + \boldsymbol{G}(q). \tag{49}$$

In this paper, the dynamic model of the 2PRU-UPR parallel robot is rewritten as

$$\boldsymbol{H}^T \boldsymbol{M}_I \boldsymbol{H}\ddot{\boldsymbol{q}} + \boldsymbol{H}^T \boldsymbol{C}(q, \dot{q}) = \boldsymbol{H}^T \boldsymbol{F}^a, \tag{50}$$

where $\boldsymbol{H} = \begin{bmatrix} \boldsymbol{J}_R & \boldsymbol{J}_T \end{bmatrix}^T$ is a 36×3 matrix comprising the rotation matrix and translation matrix of the corresponding parts of the parallel robot, $\boldsymbol{M}_I = \begin{bmatrix} \boldsymbol{I} & \boldsymbol{0} \\ \boldsymbol{0} & \boldsymbol{m} \end{bmatrix}$ is the 36×36 mass inertia matrix, and $\boldsymbol{F}^a$ denotes external forces or torques applied to the parallel mechanism. The forces and torques are the gravitational forces of all bodies, the driving forces of the

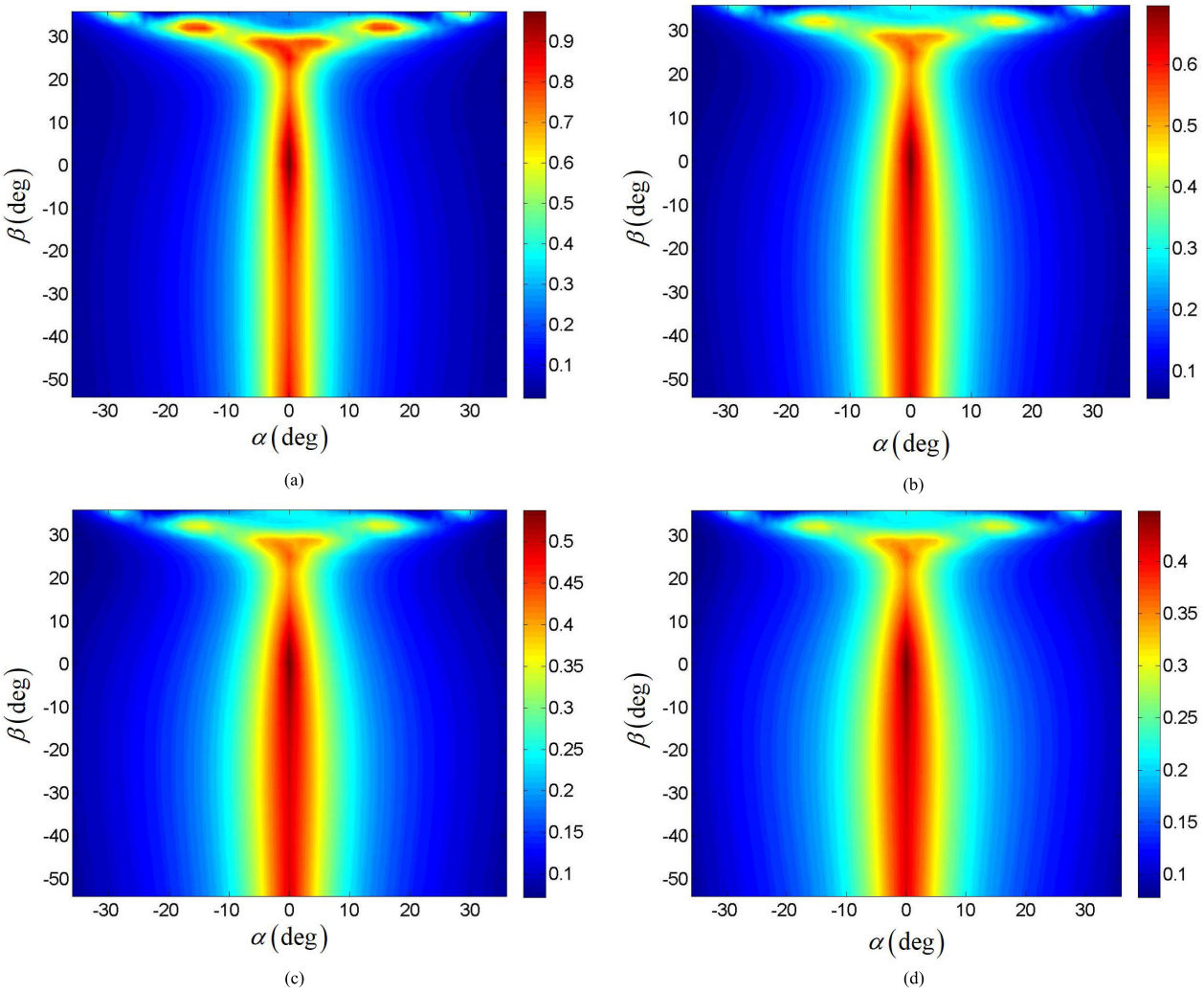

FIGURE 4. Dynamic index of rotation for different values of z. (a) DME for rotation with $z = 0.1$ m. (b) DME for rotation with $z = 0.14$ m. (c) DME for rotation with $z = 0.18$ m. (d) DME for rotation with $z = 0.22$ m.

prismatic joints, the loads applied to the moving platform and the related torques.

For the 2PRU-UPR parallel robot, we rewrite (50) in the form

$$\boldsymbol{J}_d^{-T}\boldsymbol{H}^T\boldsymbol{M}_I\boldsymbol{H}\boldsymbol{J}_e^{+}\left(\dot{\tilde{\boldsymbol{v}}}_e-\dot{\boldsymbol{J}}_e\dot{\boldsymbol{q}}\right)=\boldsymbol{F}_d+\boldsymbol{J}_d^{-T}\left(\boldsymbol{F}_a-\boldsymbol{C}\right), \quad (51)$$

where $\boldsymbol{F}_d$ is the driving force applied to the sliders of the parallel robot. The 3×3 matrix $\boldsymbol{J}_d$ is related to the system's generalized coordinates; i.e., $\dot{d} = \boldsymbol{J}_d\dot{q}$. The vector $\dot{\tilde{\boldsymbol{v}}}_e = \left[\dot{\boldsymbol{\omega}}_P^T\ \dot{\boldsymbol{v}}_P^T\right]^T$ denotes the rotational and translational accelerations of the end-effector of the parallel mechanism. The 6×3 matrix $\boldsymbol{J}_e = \boldsymbol{J}_P = [\boldsymbol{J}_{P,R}^T\ \boldsymbol{J}_{P,T}^T]^T$ is the Jacobian of the parallel mechanism's end-effector.

According to (51), a dynamic manipulability ellipsoid is obtained to describe the performance of the moving platform in terms of acceleration in various directions as

$$\| \boldsymbol{F} \| \leq 1 \Rightarrow \tilde{\boldsymbol{a}}^T\tilde{\boldsymbol{J}}^{+T}\tilde{\boldsymbol{M}}^T\tilde{\boldsymbol{M}}\tilde{\boldsymbol{J}}^{+}\tilde{\boldsymbol{a}} \leq 1, \quad (52)$$

where $\tilde{\boldsymbol{a}} = \dot{\tilde{\boldsymbol{v}}}_e - \dot{\boldsymbol{J}}_e\dot{\boldsymbol{q}}$ is the acceleration of the moving platform. $\tilde{\boldsymbol{M}} = \boldsymbol{J}_d^{-T}\boldsymbol{H}^T\boldsymbol{M}_I\boldsymbol{H}\boldsymbol{J}_d^{-1}$ is a 3×3 inertia matrix of the parallel mechanism, and $\tilde{\boldsymbol{J}} = \boldsymbol{J}_e\boldsymbol{J}_d^{-1}$ is a 6×3 matrix.

A separate dynamic matrix associated with the rotation and translation of the manipulator is derived from (52). By replacing the corresponding parts of the Jacobian matrix with separate parts, two dynamics manipulability ellipsoids are obtained for the evaluation of the performances of rotational and translational accelerations:

$$\begin{aligned}\tilde{\boldsymbol{a}}_R^T\tilde{\boldsymbol{J}}_R^{+T}\tilde{\boldsymbol{M}}^T\tilde{\boldsymbol{M}}\tilde{\boldsymbol{J}}_R^{+}\tilde{\boldsymbol{a}}_R &\leq 1\\ \tilde{\boldsymbol{a}}_T^T\tilde{\boldsymbol{J}}_T^{+T}\tilde{\boldsymbol{M}}^T\tilde{\boldsymbol{M}}\tilde{\boldsymbol{J}}_T^{+}\tilde{\boldsymbol{a}}_T &\leq 1,\end{aligned} \quad (53)$$

where $\tilde{\boldsymbol{a}}_R$ and $\tilde{\boldsymbol{a}}_T$ are related to the rotational and translational aspects of $\tilde{\boldsymbol{a}}$, respectively. Accordingly, the separate Jacobians are given by $\tilde{\boldsymbol{J}}_R = \boldsymbol{J}_{P,R}\boldsymbol{J}_d^{-1}$ and $\tilde{\boldsymbol{J}}_T = \boldsymbol{J}_{P,T}\boldsymbol{J}_d^{-1}$, both of which are 3×3 matrices.

It is found from (7) that coordinate y is related to coordinate z. Combined with the mobility characteristic of the

FIGURE 5. Prototype of the parallel robot.

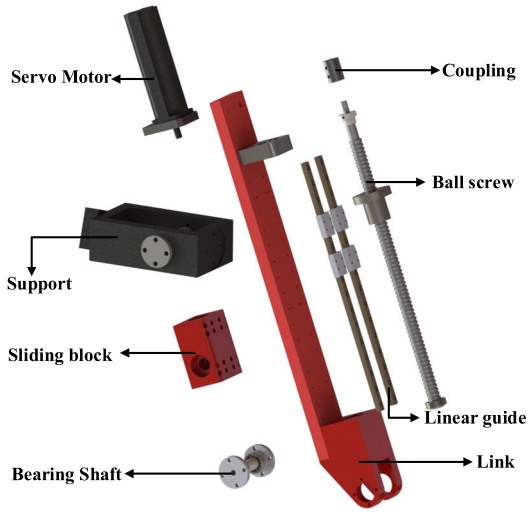

FIGURE 6. Exploded view of a UPR limb.

2PRU-UPR parallel robot, the ellipsoids described by (53) can be understood as a two-dimensional subspace of a three-dimensional rotational space and a two-dimensional subspace of a three-dimensional translational space. The rotational and translational accelerations are therefore limited to two different planes. On this basis, both $\tilde{\boldsymbol{J}}_R^{+T}\tilde{\boldsymbol{M}}^T\boldsymbol{M}\,\tilde{\boldsymbol{J}}_R^{+}$ and $\tilde{\boldsymbol{J}}_T^{+T}\tilde{\boldsymbol{M}}^T\boldsymbol{M}\,\tilde{\boldsymbol{J}}_T^{+}$ are symmetric semidefinite matrices with rank 2, and each has two positive eigenvalues and one zero eigenvalue. Using these nonzero eigenvalues, the condition number of the 3×3 matrix $\boldsymbol{M}\,\tilde{\boldsymbol{J}}_R^{+}$ is used to evaluate the isotropic characteristics of rotation in the dynamic performance of manipulators:

$$\omega_R = \frac{\sigma_{R,1}}{\sigma_{R,2}}, \tag{54}$$

where $\sigma_{R,1}$ and $\sigma_{R,2}$ are nonzero singular values of $\tilde{M}\tilde{J}_R^{+}$ and $\sigma_{R,1} \leq \sigma_{R,2}$. Similarly, the translation in the dynamic performance of manipulators is

$$\omega_T = \frac{\sigma_{T,1}}{\sigma_{T,2}}, \tag{55}$$

where $\sigma_{T,1}$ and $\sigma_{T,2}$ are nonzero singular values of $\tilde{M}\tilde{J}_T^{+}$ and $\sigma_{T,1} \leq \sigma_{T,2}$.

Kinematics analysis reveals that parameters α, β and z affect the dynamic manipulability. Hence, in the performance analysis, the DME is analyzed using α, β and z. The dynamic index of translation is affected by the parameter z, which increases from 0.1 to 0.22 m, as shown in Fig. 3(a)–(d). The dynamic index of rotation is also affected by parameter z, as shown in Fig. 4(a)–(d).

Figure 3(a)–(d) shows the DME for the manipulator at its highest position. In this case, the manipulator is asymmetrical around the α axis, which can be explained in that the translation is only associated with the first and second limbs. The third limb contributes nothing to the translation. The model is symmetrical along the α axis but asymmetrical along the β axis. With z increasing from 0.1 to 0.22 m, the range of the DME index in the direction of the β axis increases and the distribution moves along the β axis. The reason may be that with z increasing from 0.1 to 0.22 m, the angles of the third limb and moving platform are smaller when the moving platform is parallel to the fixed base. Figure 3(a)–(d) also shows that when $\alpha > 30°$, $\alpha < -30°$ or $\beta > 30°$, the translational dynamic performance is poor owing the 2PRU-UPR parallel robot being near the singular configurations in these regions. Additionally, the maximum value of the translational performance increases from 0.45 to 0.7 with z increasing from 0.1 to 0.22 m, which means that a better range for translational operations is around $z = 0.22$m.

Figure 4(a)–(d) shows the manipulator at two higher positions with symmetry along the α axis. The two higher positions are achieved as a result of the positions of the limbs. Rotation around the α axis is only associated with the first and second limbs while rotation around the β axis is only associated with the third limb. As the model is symmetrical along the α axis and asymmetrical along the β axis, the dynamic index of rotation is symmetrical along the α axis and asymmetrical along the β axis. With an increase in z from 0.1 to 0.22 m, the distance between the manipulator and driving pairs lengthens, leading to a smaller dynamic index for rotation. Figure 4(a)–(d) also shows that the rotational dynamic performance is poor when $\alpha > 5°$ or $\alpha < -5°$. In contrast with the distributions of translational dynamic performances, the maximum value of the index of rotational performance decreases from 0.9 to 0.45 with z increasing from 0.1 to 0.22 m, which means that the better region for industrial application (i.e., the better range for rotational operations) is around $z = 0.1$m. Figures 3 and 4 show that it is necessary to select different operational ranges according to the actual needs of rotation and translation in future applications.

VII. PROTOTYPING

A prototype of the 2PRU-UPR parallel robot has been built, as shown in Fig. 5. An exploded diagram of the UPR limb is shown in Fig. 6. Each limb comprises a support frame,

linear units and links connected by revolute joints, as shown in the figure. A linear unit includes a servo motor (ECMA-C10401FS), a link, ball screws (R16-5T3-FSI), couplings, a linear guide (MGN9C-2-R315-Z0-H-M), a support, a bearing shaft and a sliding block. The key link parameters were introduced in Section 5. To guarantee the workspace and avoid a singularity, the displacement of the prismatic pairs is limited within a certain range $d_i \in [75mm,\ 310mm]$, and the screw length and lead are set at 400 and 5 mm, respectively. To prevent the sliding block from breaking, two optoelectronic switches are installed near the two ends of the screw. When the sliding block is detected by the optoelectronic switch, the control system stops the movement of the corresponding servo motor. Experiments on the dynamics, accuracy and kinematic calibration will be conducted in future work.

VIII. CONCLUSION

The dynamic modeling and performance analysis of a 3-DOF 2PRU-UPR parallel robot were presented. On the basis of inverse kinematics, expressions of the velocity and acceleration of joints and limbs of the 2PRU-UPR parallel robot were easily derived using screw theory, and the actuated forces were then obtained directly using the principle of virtual work. The proposed modeling method was verified in numerical simulation against dynamics modeling using ADAMS software. The DME was used to evaluate the dynamic translational and rotational performances of the 2PRU-UPR parallel robot, and the effects of the operating height on the distribution of the DME were discussed in detail, providing criteria for further precise control and high-speed machining. A prototype suitable for the machining of curved surfaces was built.

REFERENCES

[1] H. Asada, "A geometrical representation of manipulator dynamics and its application to arm design," *J. Dyn. Syst., Meas., Control*, vol. 105, no. 3, pp. 131–142, Sep. 1983.

[2] T. Yoshikawa, "Dynamic manipulability of robot manipulators," in *Proc. IEEE Int. Conf. Robot. Automat. (ICRA)*, Mar. 1985, pp. 1033–1038.

[3] O. Khatib, "Inertial properties in robotic manipulation: An object-level framework," *Int. J. Robot. Res.*, vol. 14, no. 1, pp. 19–36, Jul. 2016.

[4] R. Kurazume and T. Hasegawa, "A new index of serial-link manipulator performance combining dynamic manipulability and manipulating force ellipsoids," *IEEE Trans. Robot.*, vol. 22, no. 5, pp. 1022–1028, Oct. 2006.

[5] Y. L. Kuo, W. L. Cleghorn, and K. Behdinan, "Stress-based finite element method for Euler-Bernoulli beams," *Trans. Can. Soc. Mech. Eng.*, vol. 30, no. 1, pp. 1–6, Mar. 2006.

[6] S. K. Dwivedy and P. Eberhard, "Dynamic analysis of flexible manipulators, a literature review," *Mechanism Mach. Theory*, vol. 41, no. 7, pp. 749–777, Jul. 2006.

[7] H. D. Taghirad, *Parallel Robots: Mechanics and Control*. Boca Raton, FL, USA: CRC Press, 2013.

[8] I. T. Pietsch, M. Krefft, O. T. Becker, C. C. Bier, and J. Hesselbach, "How to reach the dynamic limits of parallel robots? An autonomous control approach," *IEEE Trans. Autom. Sci. Eng.*, vol. 2, no. 4, pp. 369–380, Oct. 2005.

[9] A. Izadbakhsh, "Closed-form dynamic model of PUMA 560 robot arm," in *Proc. 4th Int. Conf. Auto. Robots Agents (ICARA)*, Feb. 2009, pp. 675–680.

[10] Y. Wu and C. Gosselin, "Design of reactionless 3-DOF and 6-DOF parallel manipulators using parallelepiped mechanisms," *IEEE Trans. Robot.*, vol. 21, no. 5, pp. 821–833, Oct. 2005.

[11] J. G. Wang and C. M. Gosselin, "A new approach for the dynamic analysis of parallel manipulators," *Multibody. Syst. Dyn.*, vol. 2, no. 3, pp. 317–334, Sep. 1998.

[12] B. Dasgupta and T. S. Mruthyunjaya, "A Newton-euler formulation for the inverse dynamics of the stewart platform manipulator," *Mechanism Mach. Theory*, vol. 33, no. 8, pp. 1135–1152, Nov. 1998.

[13] A. De Luca and L. Ferrajoli, "A modified Newton-euler method for dynamic computations in robot fault detection and control," in *Proc. IEEE Int. Conf. Robot. Autom.*, May 2009, pp. 3359–3364.

[14] G. Chen, W. Yu, Q. Li, and H. Wang, "Dynamic modeling and performance analysis of the 3-PRRU 1T2R parallel manipulator without parasitic motion," *Nonlinear Dyn.*, vol. 90, no. 1, pp. 339–353, Jul. 2017.

[15] Z. Wang, N. Zhang, X. Chai, and Q. Li, "Kinematic/dynamic analysis and optimization of a 2-URR-RRU parallel manipulator," *Nonlinear Dyn.*, vol. 88, no. 1, pp. 503–519, Dec. 2016.

[16] S. Herrero, C. Pinto, O. Altuzarra, and M. Diez, "Analysis of the 2PRU-1PRS 3DOF parallel manipulator: Kinematics, singularities and dynamics," *Robot. Comput-Integr. Manuf.*, vol. 51, pp. 63–72, Jun. 2018.

[17] H. Abdellatif and B. Heimann, "Computational efficient inverse dynamics of 6-DOF fully parallel manipulators by using the lagrangian formalism," *Mechanism Mach. Theory*, vol. 44, no. 1, pp. 192–207, Jan. 2009.

[18] Y. K. Yiu, H. Cheng, Z. H. Xiong, G. F. Liu, and Z. X. Li, "On the dynamics of parallel manipulators," in *Proc. IEEE Int. Conf. Robot. Automat. (ICRA)*, May 2001, pp. 3766–3771.

[19] J. Yao, W. Gu, Z. Feng, L. Chen, Y. Xu, and Y. Zhao, "Dynamic analysis and driving force optimization of a 5-DOF parallel manipulator with redundant actuation," *Robot. Comput.-Integr. Manuf.*, vol. 48, pp. 51–58, Dec. 2017.

[20] C. Zhu, J. Katupitiya, and J. Wang, "Effect of links deformation on motion precision of parallel manipulator based on flexible dynamics," *Ind. Robot, Int. J.*, vol. 44, no. 6, pp. 776–787, Oct. 2017.

[21] T. Sun, D. Liang, and Y. Song, "Singular-Perturbation-Based nonlinear hybrid control of redundant parallel robot," *IEEE Trans. Ind. Electron.*, vol. 65, no. 4, pp. 3326–3336, Apr. 2018.

[22] L.-W. Tsai, "Solving the inverse dynamics of a stewart-gough manipulator by the principle of virtual work," *J. Mech. Design*, vol. 122, no. 1, pp. 3–9, Dec. 1999.

[23] Y. Zhao and F. Gao, "Inverse dynamics of the 6-dof out-parallel manipulator by means of the principle of virtual work," *Robotica*, vol. 27, no. 2, pp. 259–268, Mar. 2009.

[24] H. Kalani, A. Rezaei, and A. Akbarzadeh, "Improved general solution for the dynamic modeling of Gough–Stewart platform based on principle of virtual work," *Nonlinear Dyn.*, vol. 83, no. 4, pp. 2393–2418, Nov. 2015.

[25] Y. Zhao, Z. Zhang, and G. Cheng, "Inverse rigid-body dynamic analysis for a 3UPS-PRU parallel robot," *Adv. Mech. Eng.*, vol. 9, no. 2, Feb. 2017, Art. no. 168781401769319.

[26] Y. Qi and Y. Song, "Coupled kinematic and dynamic analysis of parallel mechanism flying in space," *Mechanism Mach. Theory*, vol. 124, pp. 104–117, Jun. 2018.

[27] M. Díaz-Rodríguez, V. Mata, Á. Valera, and Á. Page, "A methodology for dynamic parameters identification of 3-DOF parallel robots in terms of relevant parameters," *Mechanism Mach. Theory*, vol. 45, no. 9, pp. 1337–1356, Sep. 2010.

[28] A. M. Shafei and H. R. Shafei, "Dynamic modeling of planar closed-chain robotic manipulators in flight and impact phases," *Mechanism Mach. Theory*, vol. 126, pp. 141–154, Aug. 2018.

[29] R. M. M. Orsino, T. A. H. Coelho, and C. P. Pesce, "Analytical mechanics approaches in the dynamic modelling of delta mechanism," *Robotica*, vol. 33, no. 4, pp. 953–973, Mar. 2014.

[30] S. Wen, H. Yu, B. Zhang, Y. Zhao, H. K. Lam, G. Qin, and H. Wang, "Fuzzy identification and delay compensation based on the Force/Position control scheme of the 5-DOF redundantly actuated parallel robot," *Int. J. Fuzzy Syst.*, vol. 19, no. 1, pp. 124–140, Mar. 2016.

[31] L. Carbonari, M. Battistelli, M. Callegari, and M.-C. Palpacelli, "Dynamic modelling of a 3-CPU parallel robot via screw theory," *Mech. Sci.*, vol. 4, no. 1, pp. 185–197, Apr. 2013.

[32] J. Gallardo, J. M. Rico, A. Frisoli, D. Checcacci, and M. Bergamasco, "Dynamics of parallel manipulators by means of screw theory," *Mechanism Mach. Theory*, vol. 38, no. 11, pp. 1113–1131, Nov. 2003.

[33] J. M. Rico, J. Gallardo, and J. Duffy, "Screw theory and higher order kinematic analysis of open serial and closed chains," *Mechanism Mach. Theory*, vol. 34, no. 4, pp. 559–586, May 1999.
[34] J. Gallardo-Alvarado, C. R. Aguilar-Nájera, L. Casique-Rosas, L. Pérez-González, and J. M. Rico-Martínez, "Solving the kinematics and dynamics of a modular spatial hyper-redundant manipulator by means of screw theory," *Multibody Syst. Dyn.*, vol. 20, no. 4, pp. 307–325, Sep. 2008.
[35] J. Gallardo-Alvarado, R. Rodríguez-Castro, and P. J. Delossantos-Lara, "Kinematics and dynamics of a 4- p RUR Schönflies parallel manipulator by means of screw theory and the principle of virtual work," *Mechanism Mach. Theory*, vol. 122, pp. 347–360, Apr. 2018.
[36] J. C. M. Carvalho and M. Ceccarelli, "A closed-form formulation for the inverse dynamics of a Cassino parallel manipulator," *Multibody. Syst. Dyn.*, vol. 5, no. 2, pp. 185–210, Oct. 2001.
[37] L. F. Kong, S. H. Zhang, W. H. Xiao, C. Y. Li, and Z. Huang, "Rigid body dynamics model of the 6-PUS parallel mechanism based on Newton-Euler method," *Robot*, vol. 26, no. 5, pp. 395–399, Sep. 2004.
[38] Y. Li and Q. Xu, "Kinematics and inverse dynamics analysis for a general 3-PRS spatial parallel mechanism," *Robotica*, vol. 23, no. 2, pp. 219–229, Mar. 2005.
[39] L. Xu, X. Zhu, W. Ye, Q. Li, and Q. Chen, "Kinematic analysis and dimensional synthesis of a new 2R1T parallel kinematic machine," in *Proc. 42nd Mech. Robot. Conf.*, Nov. 2018, pp. 1–9.
[40] K. Neumann, "Robot," U.S. Patent 4 732 525, Mar. 22, 1988.
[41] Z. M. Bi and Y. Jin, "Kinematic modeling of exechon parallel kinematic machine," *Robot. Comput.-Integr. Manuf.*, vol. 27, no. 1, pp. 186–193, Feb. 2011.
[42] K. L. Doty, C. Melchiorri, E. M. Schwartz, and C. Bonivento, "Robot manipulability," *IEEE Trans. Robot. Autom.*, vol. 11, no. 3, pp. 462–468, Jun. 1995.
[43] P. Chiacchio, "A new dynamic manipulability ellipsoid for redundant manipulators," *Robotica*, vol. 18, no. 4, pp. 381–387, Apr. 2001.
[44] Y. Yokokohji, J. San Martin, and M. Fujiwara, "Dynamic manipulability of multifingered grasping," *IEEE Trans. Robot.*, vol. 25, no. 4, pp. 947–954, Aug. 2009.

XINXUE CHAI received the B.S. and Ph.D. degrees in mechanical engineering from Zhejiang Sci-Tech University, Hangzhou, China, in 2011 and 2017, respectively.

Since 2017, she has been a Lecturer with the Faculty of Mechanical Engineering and Automation, Zhejiang Sci-Tech University. Her research interest includes mechanism theory using geometric algebra.

MIN WANG received the B.S. degree in mechanical engineering and automatics from the Jiangsu University of Science and Technology, Zhenjiang, China, in 2017.

His research interest includes dynamic modelling of parallel mechanisms.

LINGMIN XU (Member, IEEE) received the B.S. degree in mechanical engineering from Zhejiang Sci-Tech University, Hangzhou, China, in 2015, where he is currently pursuing the Ph.D. degree with the Faculty of Mechanical Engineering and Automation.

From 2018 to 2019, he was a Visiting Graduate Student with The University of Illinois at Chicago, Chicago, IL, USA. His main research interests include kinematics and dynamics of parallel robots.

WEI YE (Member, IEEE) received the B.S. and Ph.D. degrees in mechanical engineering from Beijing Jiaotong University, Beijing, China, in 2010 and 2016, respectively.

He joined the Faculty of Mechanical Engineering and Automation, Zhejiang Sci-Tech University, in 2016, where he is currently a Lecturer. He is the author of one book and more than 20 articles. His research interests include mechanism theory and application of parallel manipulators.